

Orbital-selective Mott Phase in Multiorbital Models for Alkaline Iron Selenides $K_{1-x}Fe_{2-y}Se_2$

Rong Yu¹ and Qimiao Si¹

¹*Department of Physics & Astronomy, Rice University, Houston, Texas 77005*

We study a multiorbital model for the alkaline iron selenides $K_{1-x}Fe_{2-y}Se_2$ using a slave-spin method. With or without ordered vacancies, we identify a metal-to-Mott-insulator transition at the commensurate filling of six 3d electrons per iron ion. For Hund's couplings beyond a threshold value, this occurs via an intermediate orbital-selective Mott phase, in which the 3d xy orbital is Mott localized while the other 3d orbitals remain itinerant. This phase is still stabilized over a range of carrier dopings. Our results lead to an overall phase diagram for the alkaline iron selenides, which provides a unified framework to understand the interplay between the strength of vacancy order and carrier doping. In this phase diagram, the orbital-selective Mott phase provides a natural link between the superconducting $K_{1-x}Fe_{2-y}Se_2$ and its Mott-insulating parent compound.

Introduction. An important question of active discussions is the strength of the electron correlations in iron-based superconductors [1, 2]. The issue is crucial for understanding the properties of both the normal and superconducting states of these systems. For the iron pnictides, the antiferromagnetically ordered metallic ground state of the parent compounds [3] may arise either from the Fermi surface nesting of a weak coupling theory [4, 5], or from the strong correlation effects associated with the proximity to a Mott transition and the concomitant quasi-local moments [6–12]. A number of factors argue in favor of the latter picture, including the large spectral weight in the fluctuating magnetic spectrum [13]. For the 11 iron chalcogenides [14], both the large ordered magnetic moment and the ordering wave vector are difficult to understand within the nesting picture. Also pertinent is the iron oxychalcogenide $La_2O_3Fe_2Se_2$, in which the Mott insulating behavior has been experimentally identified and theoretically explained in terms of the band narrowing effect associated with the expansion of the iron lattice unit cell [15]. These results suggest that the incipient Mott picture [16, 17] is even more pronounced in the iron chalcogenides.

The recently discovered alkaline iron selenide superconductors [18] $A_{1-x}Fe_{2-y}Se_2$ ($A=K, Rb, Cs, \text{ or } Tl$) shed new light on this issue. In these materials the superconducting T_c is comparable to that of the pnictides [18–21], and the superconductivity is near an insulating phase [22, 23]. The insulator is antiferromagnetic with a very large ordered moment [24, 25], and is intimately connected to the ordered iron vacancies [22, 24, 26]. The lack of hole pockets in the Fermi surface of the superconducting compounds revealed by the ARPES measurements [27–29] makes the high T_c superconductivity and the large-moment magnetic order hardly explainable by the nesting mechanism. Instead, they are more naturally understood in terms of the incipient Mott picture. For instance, the insulating state is naturally interpreted as a Mott insulator (MI), not only because it would have been metallic in the absence of interactions but also because the interactions are strong as inferred from the large ordered moment; the enhanced interaction effects have been attributed to the band-narrowing caused by the ordered iron vacancies [30–32]. Various experiments suggest that the superconducting state is either free of iron vacancies or vacancy disordered, and

is intrinsically phase separated from the vacancy ordered insulating state [33–35]. A key open question is how the vacancy ordered insulating state connects to superconducting phase. Elucidating the linkage between the two phases is an important goal of the present study.

It is well known that tuning either correlation strength or carrier density may induce metal-to-insulator transitions (MITs) in correlated electron systems [36]. In multiorbital systems, the physics associated with this transition is richer than that of one-band systems since both the bandstructure and the correlation strength may be orbital dependent. An extreme example is the orbital-selective Mott transition (OSMT), for which the Mott transition takes place at different correlation strengths for different orbitals [37, 38]. It is believed that the OSMT occurs in $(Ca, Sr)_2RuO_4$. [37–39] For iron-based superconductors, strong orbital differences have been suggested in several systems [40–42]. For the iron pnictides, it was shown theoretically [43] that the OSMT has nearly as competitive a ground-state energy as the other competing phases but is ultimately not stabilized as a ground state.

In this letter, we investigate the MIT in the alkaline iron selenides system $K_{1-x}Fe_{2-y}Se_2$ using a slave-spin method [43, 44]. We show that when the Hund's coupling is sufficiently strong, the Mott localization of the system is always via an OSMP, in which the 3d xy orbital is Mott localized, while the other orbitals are still itinerant. This OSMP generally exists in both the iron vacancy ordered and disordered cases, and survives a range of carrier doping. It provides a necessary connection between the vacancy ordered insulating phase and the metallic normal state above T_c . Our results allow us to make contact with recent ARPES measurements in this system [45].

Model and method. We consider a multiorbital Hubbard model for the $K_{1-x}Fe_{2-y}Se_2$ compound. The Hamiltonian reads

$$H = H_0 + H_{\text{int}}. \quad (1)$$

Here, H_0 contains the tight-binding parameters among the five 3d-orbitals,

$$H_0 = \frac{1}{2} \sum_{ij\alpha\beta\sigma} t_{ij}^{\alpha\beta} d_{i\alpha\sigma}^\dagger d_{j\beta\sigma} + \sum_{i\alpha\sigma} (\epsilon_\alpha - \mu) d_{i\alpha\sigma}^\dagger d_{i\alpha\sigma}, \quad (2)$$

where $d_{i\alpha\sigma}^\dagger$ creates an electron in orbital $\alpha = 1, \dots, 5$ with spin

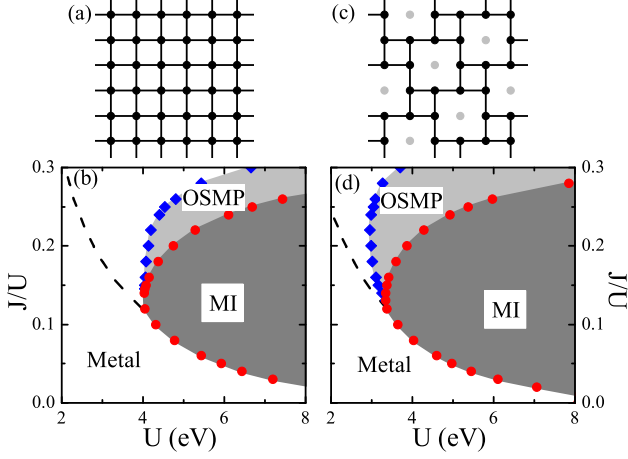


FIG. 1. (Color online) a),c): The regular and 1/5-depleted square lattices, respectively corresponding to the alkaline iron selenides with disordered and the $\sqrt{5} \times \sqrt{5}$ ordered iron vacancies. b),d): Corresponding phase diagrams in the J - U plane at commensurate filling $N = 6$ per Fe for the multiorbital model. The dark and light shaded regions respectively refer to the Mott insulator (MI) and the orbital-selective Mott phase (OSMP). The red circles and blue diamonds respectively denote the Mott transition and the crossover between the fully itinerant metal phase and OSMP. The black dashed line shows the crossover scale U^* between the weakly and strongly correlated metals.

σ at site i , ϵ_α is the on-site energy reflecting the crystal level splitting, and μ is the chemical potential. We have taken the tight-binding parameters from Ref. 45, and the units are in eV. H_{int} contains on-site Coulomb interactions

$$\begin{aligned}
 H_{\text{int}} = & \frac{U}{2} \sum_{i,\alpha,\sigma} n_{i\alpha\sigma} n_{i\alpha\bar{\sigma}} \\
 & + \sum_{i,\alpha<\beta,\sigma} \{ U' n_{i\alpha\sigma} n_{i\beta\bar{\sigma}} + (U' - J) n_{i\alpha\sigma} n_{i\beta\sigma} \\
 & - J (d_{i\alpha\sigma}^\dagger d_{i\alpha\bar{\sigma}} d_{i\beta\bar{\sigma}}^\dagger d_{i\beta\sigma} - d_{i\alpha\sigma}^\dagger d_{i\alpha\bar{\sigma}}^\dagger d_{i\beta\bar{\sigma}} d_{i\beta\sigma}) \}. \quad (3)
 \end{aligned}$$

where $n_{i\alpha\sigma} = d_{i\alpha\sigma}^\dagger d_{i\alpha\sigma}$. In this model, U , U' , and J respectively denote the intraorbital repulsion, interorbital repulsion, and Hund's rule exchange coupling. We will take $U' = U - 2J$. [46]

The MIT of the above model is studied using a $U(1)$ slave-spin method [43]. Here, a slave $S=1/2$ quantum spin is introduced to carry the charge degree of freedom, and the metallic (Mott insulating) state corresponds to the magnetically (dis)ordered state of the slave spins with quasiparticle spectral weight in each orbital $Z_\alpha > 0$ ($Z_\alpha = 0$). For simplicity, in the calculation we drop the spin-flip and pair-hopping terms in the interaction H_{int} . Including these terms leads to similar results [40]. We study the MIT on two two-dimensional (2D) lattices of iron ions: a regular square lattice sketched in Fig. 1(a) and a 1/5-depleted square lattice shown in Fig. 1(c). They respectively stand for the completely disordered and the perfect $\sqrt{5} \times \sqrt{5}$ iron vacancies.

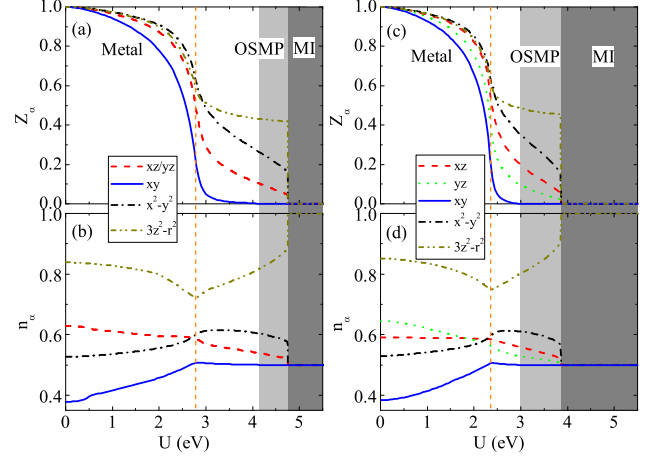


FIG. 2. (Color online) (a) and (b): Evolution of orbital resolved quasiparticle spectral weight Z_α (in (a)) and orbital filling factor (per iron site per spin) with U for the multiorbital model at $N = 6$ and $J/U = 0.2$ on the regular lattice. The vertical dashed line indicates the position of U^* , which specifies the dashed lines in Fig. 1(b)(d). (c) and (d): Same as (a) and (b) but on one of the two inequivalent sites of a unit cell of the 1/5-depleted lattice. Z_α for the xz and yz orbitals switch on the other site, as do the orbital filling factors.

Metal-to-insulator transition. The results at the commensurate filling corresponding to $N = 6$ 3d electrons per Fe are summarized in the phase diagrams of Figs. 1(b) and (d). In both the vacancy disordered and ordered cases, the system experiences a Mott transition at U_{MT} from a metal to a MI with increasing U . The insulating phase is a low-spin MI for $J/U \lesssim 0.01$, but a $S=2$ high-spin MI for larger J values. U_{MT} first decreases then increases with increasing J/U ratio. Such a nonmonotonic behavior is a general feature of systems away from one electron per orbital, and is also obtained in the five-orbital model for the parent iron pnictides [43]. When the Hund's coupling is above a threshold ($J/U \gtrsim 0.1$), the system crosses over from a weakly correlated metal to a strongly correlated metal with increasing U . The onset of this crossover (at U^*) is identified by a rapid drop of Z_α and a kink in the orbital filling in each orbital, as shown in Figs. 2(a)-(d). In the strongly correlated metallic state, Z_α is strongly orbital dependent. Increasing U does not lead to the simultaneous Mott localization of all orbitals. The metallic state first crosses over to an intermediate OSMP at U_{OS} . The Mott transition then takes place between the MI and the OSMP at a larger U .

Importantly, the phase diagram of the vacancy ordered system is similar to that of its vacancy disordered counterpart. Quantitatively, U_{MT} and U_{OS} are respectively smaller in the vacancy ordered system, which reflects the ordered-vacancy-induced reduction in the kinetic energy and hence enhancement in the correlation effects [30].

Nature of the orbital-selective Mott phase. As shown in Figs. 2(a) and (c), in the strongly correlated metallic regime, Z in the xy orbital is suppressed the most, and this orbital is

very close to half-filling. Further increasing U results in the Mott localization of the xy orbital at U_{OS} . The other orbitals remain itinerant up to U_{MT} . The system is thus in an OSMP for $U_{OS} < U < U_{MT}$. We now turn to discussing the factors that stabilize the OSMP. For simplicity, we limit our discussion to the vacancy disordered case. The vacancy ordered case is qualitatively similar.

We start from the physics that governs the crossover between the weakly and strongly correlated metals. Fig. 3(a) plots the effective magnetic moment $S_{\text{eff}} = \sqrt{\langle (S_z)^2 \rangle}$ as a function of J/U . It rapidly increases when the system passes through the crossover. In the strongly correlated metallic phase, $S_{\text{eff}} \approx 2$, indicating that the $S = 2$ high-spin configuration, promoted by the Hund's coupling, is dominant in this regime.

The Hund's coupling also suppresses the inter-orbital correlations $C_{\alpha,\beta} = \langle n_\alpha n_\beta \rangle - \langle n_\alpha \rangle \langle n_\beta \rangle$, as shown in Fig. 3(a). Together with the crystal level splitting, this effectively decouples the xy orbital from the others because in $\text{K}_{1-x}\text{Fe}_{2-y}\text{Se}_2$ the xy orbital is the topmost level and is well separated from the others. For the same reason, it is easier to stabilize the xy orbital to be at half-filling for an overall filling of six electrons per Fe, as shown in Fig. 2(b) [and Fig. 2(d) for the vacancy-ordered case]. Compared to the degenerate xz/yz orbitals, which are also close to half-filling, the threshold value for the Mott localization in the non-degenerate xy orbital is smaller. Moreover, in the noninteracting limit the density of states (DOS) projected to the xy orbital is narrower than those of other orbitals. For instance, as shown in Fig. 3(b), the ratio of the width of DOS for the xy orbital to that for the xz/yz orbitals is about 0.6. (This is also the case for the vacancy ordered model; see the figure in the Supplementary Material.) This ratio is smaller than that for the LaOFeAs system, which is about 0.7. Hence in $\text{K}_{1-x}\text{Fe}_{2-y}\text{Se}_2$ the xy orbital contains less kinetic energy. Taking into account all the three factors, we find that in the strongly correlated metallic state, it is much easier to drive the xy orbital toward the Mott localization. The result is the OSMP.

The threshold interaction for the OSMP, U_{OS} , shows a strong dependence on J especially when J/U is large. This seems counterintuitive; one could expect that, if the xy orbital is fully decoupled from the others, U_{OS} should approach the critical U of a single-band Hubbard model, and hence should not depend on J . To understand the behavior of U_{OS} , we examine the propagation of a charge excitation by assuming both U and J are large so that we may take the ground-state configuration to be the $S = 2$ high-spin state. A charge excitation with one more electron filled in the ground state can propagate via hopping to neighboring sites. K_{xy} ($K_{\overline{xy}}$) denotes the kinetic energy gain associated with the hopping processes (not) involving the xy orbital. Two representative hopping processes that do not disturb the high-spin ground-state configuration are illustrated in Fig. 3(c). Note that $K_{xy} < K_{\overline{xy}}$, not only because the xy orbital has a narrower (non-interacting) bandwidth but also because

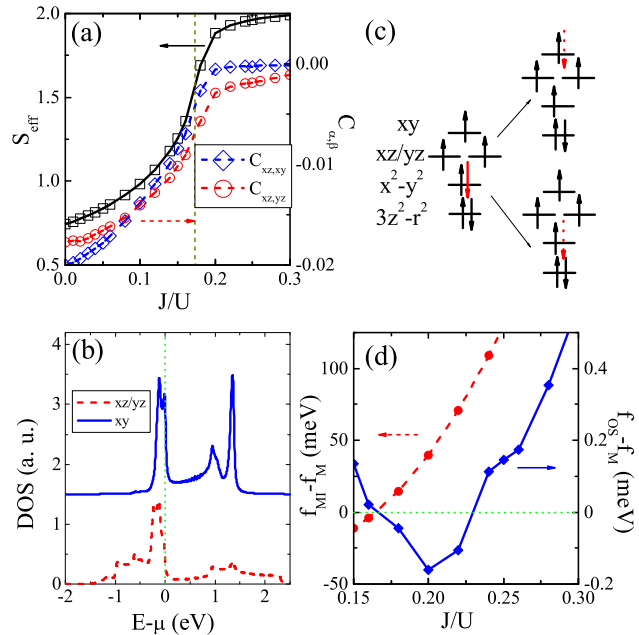


FIG. 3. (Color online) (a): Evolution of the effective moment S_{eff} and interorbital correlations $C_{xz,xy}$ and $C_{xz,yz}$ with J/U at $N = 6$ and $U = 3$ eV on the regular lattice. The vertical dashed line indicates the position of $U^*(J)$. (b): Orbital projected density of states in xy and xz/yz orbitals at the noninteracting limit ($J=U=0$) of the same model. The curve for the xy orbital is shifted upward for clarity. (c): Sketch of the two hopping processes of a charge excitation on the high-spin ground-state configuration that avoid penalty from the repulsive interactions. (d): The differences in free energy density as a function of J/U at $U = 4.2$ eV, showing the competition among the metallic (M), Mott insulating (MI), and orbital-selective Mott (OS) solutions.

the Hund's coupling suppresses the interorbital fluctuations. The Mott gap associated with either process is estimated as $\Delta_a = E(N+1) + E(N-1) - 2E(N) \approx U - 3J - K_a$, where $a = xy, \overline{xy}$. The difference in the kinetic energy gains leads to two different Mott gaps. U_{OS} (U_{MT}) can be estimated as the U value where the Mott gap Δ_a vanishes. Hence we have $U_{OS} \sim K_{xy}/(1 - 3J/U)$ and $U_{MT} \sim K_{\overline{xy}}/(1 - 3J/U)$, both of which increase with J/U . This general consideration is consistent with our calculated phase boundaries for sufficiently large J/U . Interestingly, in this regime, increasing J at a fixed U leads to a delocalization from MI to OSMP, and then to the metallic phase. This is further confirmed by comparing the free energies of the three states, as shown in Fig. 3(d). Note that in the metallic phase, the inter-orbital correlations between the xy orbital and others are substantially suppressed, but remain nonzero. The above argument on the behavior of U_{OS} does not hold for smaller J/U where U_{OS} is close to U^* . In this regime, since the ground state mixes both high- and low-spin configurations, several mechanisms favoring either increasing or decreasing U_{OS} compete. As a result,

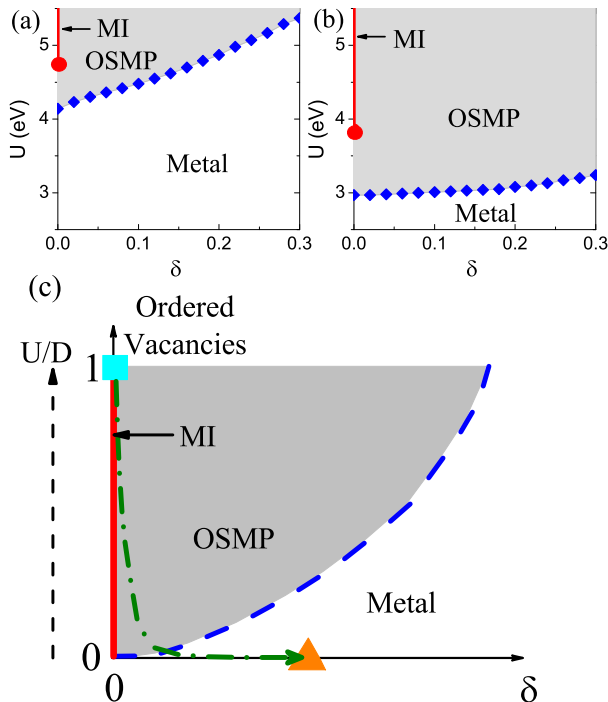


FIG. 4. (Color online) (a) and (b): Phase diagrams with U and carrier doping concentration δ for the multi-orbital model at $J/U = 0.2$ on the regular (in (a)) and the $1/5$ -depleted (in (b)) lattices, respectively. In either diagram, the large red dot refers to the Mott transition, and the blue diamonds shows the orbital-selective Mott transition. (c): Sketch of a material-based phase diagram in the plane of carrier doping δ and ordered vacancies. The vacancy order parameter has been scaled to be between 0 and 1 (see text). The vacancy ordered insulating state is located as the cyan square in this phase diagram. The superconducting state is tentatively placed as the orange triangle on the δ axis. The dash-dot line shows a possible route to connect the two phases. For realistic parameters, the Mott transition point is close to the origin, but could be either above or below it.

U_{OS} shows complicated, even nonmonotonic, J dependence (Fig. 1(b)).

Orbital-selective Mott phase at finite dopings. Unlike the MI, which exists only at a commensurate filling, the OSMF can be stabilized at incommensurate fillings if the chemical potential of the itinerant carriers falls inside the Mott gap of the localized orbital. In Figs. 4(a) and (b) we show the U vs. carrier doping concentration ($\delta = N - 6$) phase diagrams for both the vacancy disordered and ordered cases. In both systems, the Mott transition takes place between a MI and an OSMF at the commensurate filling $\delta = 0$, and an OSMT between the OSMF and the metal extends to nonzero doping concentrations. In the vacancy ordered case, both the Mott transition and the OSMT take place at lower U values compared to the vacancy disordered case, reflecting the enhanced correlations due to ordered vacancies.

Unified phase diagram for alkaline iron selenides. In light

of the above two phase diagrams, we propose a material-based unified phase diagram for both the vacancy ordered and disordered compounds. In this diagram, sketched in Fig. 4(c), the horizontal axis refers to the carrier doping δ , and the vertical axis stands for the strength of the vacancy order. In general, an $K_{1-x}Fe_{2-y}Se_2$ system contains both vacancy ordered and disordered regimes. We may parameterize the strength of the vacancy order from 0 to 1, according to the volume fraction of the vacancy ordered regime (or, alternatively, to the potential strength of a virtual Fe atom, with the vacancy corresponding to an infinite potential). The two limiting cases along the vertical axis in the phase diagram, 0 and 1, are obtained from Figs. 4(a) and (b) at a fixed U (which takes the value in real materials), respectively. The remaining part of the phase diagram can then be constructed by interpolating between the results in Figs. 4(a) and (b) at the same U . The resulting diagram consists of a MI, an OSMF, and a metallic phase. The profile is similar to what are shown in Figs. 4(a) and (b) because, effectively, the ordered vacancies enhance the correlation U/D . (Here D is a characteristic bandwidth of the multi-orbital system.) The insulating compound with the $\sqrt{5} \times \sqrt{5}$ vacancy order is located at $\delta = 0$ and vacancy order 1 (square cyan symbol in Fig. 4(c)). On the other hand, we tentatively place the superconducting phase of the superconducting compounds at ambient pressure to be on the δ axis in the metallic state close to the OSMT (triangular orange symbol in Fig. 4(c)). We see that one physical trajectory going from the insulating phase to the superconducting one is for the dopants to both introduce extra carriers and suppress the vacancy order. During the evolution of the system, the OSMF is an unavoidable intermediate phase connecting the insulating and superconducting states. A recent ARPES measurement [45] has provided evidence that the superconducting phase of $K_{1-x}Fe_{2-y}Se_2$ is indeed close to the OSMT.

In summary, we have studied the metal-to-insulator transition in the five-orbital Hubbard model for the alkaline iron selenides $K_{1-x}Fe_{2-y}Se_2$ with and without ordered vacancies. We find that the Mott localization of the system is via an intermediate orbital-selective Mott phase, in which the 3d xy orbital is localized while the other 3d orbitals are itinerant. The orbital-selective phase is stabilized by the combined effect of the orbital dependence in the bandwidths and the pinning of the xy orbital to half-filling due to both the Hund's coupling and crystal level splittings. It persists over a range of carrier dopings. Finally, we have proposed a unified phase diagram for the alkaline iron selenides, with the orbital-selective Mott phase providing the link between the insulating and superconducting compounds.

We thank Z. K. Liu, D. H. Lu, Z. X. Shen, L. L. Sun, and M. Yi for useful discussions. This work has been supported by the NSF Grant No. DMR-1006985 and the Robert A. Welch Foundation Grant No. C-1411. Q. S. acknowledges the hospitality of the Aspen Center for Physics (NSF Grant No. 1066293) and the Institute of Physics of Chinese Academy of Sciences. This work was reported in Ref. [47]. Complementary theoretical results on different systems using different

methods have subsequently been reported in Refs. [48, 49].

-
- [1] Y. Kamihara *et al.*, *J. Am. Chem. Soc.*, **130**, 3296 (2008).
 [2] Z. A. Ren *et al.*, *Chin. Phys. Lett.*, **25**, 2215 (2008).
 [3] C. de la Cruz *et al.*, *Nature* **453**, 899 (2008).
 [4] J. Dong, *et al.*, *Europhys. Lett.* **83**, 27006 (2008).
 [5] S. Graser *et al.*, *New J. Phys.* **11**, 025016 (2009).
 [6] Q. Si and E. Abrahams, *Phys. Rev. Lett.* **101**, 076401 (2008).
 [7] T. Yildirim, *Phys. Rev. Lett.* **101**, 057010 (2008).
 [8] F. Ma, Z.-Y. Lu, and T. Xiang, *Phys. Rev. B* **78**, 224517 (2008).
 [9] C. Fang *et al.*, *Phys. Rev. B* **77**, 224509 (2008).
 [10] C. Xu, M. Muller, and S. Sachdev, *Phys. Rev. B* **78**, 020501(R) (2008).
 [11] J. Dai *et al.* *Proc. Natl. Acad. Sci.* **106**, 4118 (2009).
 [12] G. S. Uhrig *et al.*, *Phys. Rev. B* **79**, 092416 (2009).
 [13] M. Liu *et al.*, *Nature Phys.* **8**, 376 (2012).
 [14] W. Bao, *et al.*, *Phys. Rev. Lett.* **102**, 247001 (2009).
 [15] J.-X. Zhu *et al.*, *Phys. Rev. Lett.* **104**, 216405 (2010).
 [16] Q. Si, E. Abrahams, J. Dai, and J.-X. Zhu, *New J. Phys.* **11**, 045001 (2009); Q. Si, *Nat. Phys.* **5**, 629 (2009).
 [17] K. Haule and G. Kotliar, *New J. Phys.* **11**, 025021 (2009).
 [18] J. Guo *et al.*, *Phys. Rev. B* **82**, 180520(R) (2010).
 [19] L. L. Sun *et al.*, *Nature* **483**, 67 (2012).
 [20] A. Krzton-Maziopa *et al.*, *J. Phys.: Condens. Matter* **23**, 052203 (2011).
 [21] Y. Mizuguchi *et al.*, *Appl. Phys. Lett.* **98**, 042511 (2011).
 [22] M. Fang *et al.*, *Euro. Phys. Lett.* **94**, 27009 (2011).
 [23] D. M. Wang, J. B. He, T.-L. Xia, and G. F. Chen, *Phys. Rev. B* **83**, 132502 (2011).
 [24] W. Bao *et al.*, *Chin. Phys. Lett.* **28**, 086104 (2011).
 [25] M. Wang *et al.*, *Nature Comm.* **2**, 580 (2011).
 [26] F. Ye *et al.*, *Phys. Rev. Lett.* **107**, 137003 (2011).
 [27] Y. Zhang *et al.*, *Nat. Mater.* **10**, 273 (2011).
 [28] T. Qian *et al.*, *Phys. Rev. Lett.* **106**, 187001 (2011)..
 [29] D. Mou *et al.*, *Phys. Rev. Lett.* **106**, 107001 (2011).
 [30] R. Yu, J.-X. Zhu, and Q. Si, *Phys. Rev. Lett.* **106**, 186401 (2011).
 [31] Y. Zhou, D.-H. Xu, F.-C. Zhang, and W.-Q. Chen, *Europhys. Lett.* **95**, 17003 (2011).
 [32] C. Cao and J. Dai, *Phys. Rev. B* **83**, 193104 (2011).
 [33] Z. Wang *et al.*, *Phys. Rev. B* **83**, 140505 (2011).
 [34] W. Li *et al.*, *Nat. Phys.* **8**, 126 (2012).
 [35] F. Chen *et al.*, *Phys. Rev. X* **1**, 021020 (2011).
 [36] M. Imada, A. Fujimori, and Y. Tokura, *Rev. Mod. Phys.* **70**, 1039 (1998).
 [37] V. Anisimov *et al.*, *Eur. Phys. J. B* **25**, 191 (2002).
 [38] L. de' Medici, S. R. Hassan, M. Capone, and X. Dai, *Phys. Rev. Lett.* **102**, 126401 (2009).
 [39] M. Neupane *et al.*, *Phys. Rev. Lett.* **103**, 097001 (2009).
 [40] R. Yu and Q. Si, *Phys. Rev. B* **84**, 235115 (2011).
 [41] Z. P. Yin, K. Haule, and G. Kotliar, *Nat. Mater.* **10**, 932 (2011).
 [42] L. Craco, M. S. Laad, and S. Leoni, *Phys. Rev. B* **84**, 224520 (2011).
 [43] R. Yu and Q. Si, *Phys. Rev. B* **86**, 085104 (2012).
 [44] L. de' Medici, A. Georges, and S. Biermann, *Phys. Rev. B* **72**, 205124 (2005).
 [45] M. Yi *et al.*, arXiv:1208.5192.
 [46] C. Castellani, C. R. Natoli, and J. Ranninger, *Phys. Rev. B* **18**, 4945 (1978).
 [47] R. Yu and Q. Si, "Metal-to-Insulator Transition in Multi-Orbital Models for $A_xFe_ySe_2$ ", APS March Meeting, <http://meetings.aps.org/link/BAPS.2012.MAR.Z22.13> (March, 2012).
 [48] Z. P. Yin, K. Haule, and G. Kotliar, arXiv:1206.0801.
 [49] E. Bascones, B. Valenzuela, and M. J. Calderon, arXiv:1208.1917.

SUPPLEMENTARY MATERIAL

Fig. 5 shows the orbital projected density of states (DOS) in xy and xz/yz orbitals at the noninteracting limit ($J=U=0$) of the vacancy ordered model. The DOS has been averaged over the two inequivalent sites of a unit cell. In the vacancy ordered model, the DOS in the xy orbital is narrower than those in the other Fe 3d orbitals, and the ratio of the width of DOS for the xy orbital to that for the xz/yz orbitals is about 0.6. These are both similar to the vacancy disordered model.

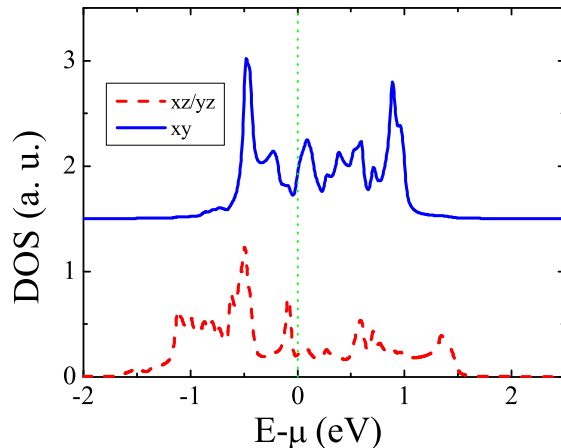


FIG. 5. (Color online) Orbital projected density of states (DOS) in xy and xz/yz orbitals at the noninteracting limit ($J=U=0$) of the vacancy ordered model at $N = 6$. The curve for the xy orbital is shifted upward for clarity. The DOS has been averaged over the two inequivalent sites of a unit cell.